Mon. Not. R. Astron. Soc. **334,** 39–47 (2002)

2016+112: a gravitationally lensed type II quasar

L. V. E. Koopmans,[1⋆] M. A. Garrett,[2] R. D. Blandford,[1]
C. R. Lawrence,[3] A. R. Patnaik[4] and R. W. Porcas[4]

[1]*California Institute of Technology, mailcode 130-33, Pasadena, CA 91125, USA*
[2]*Joint Institute for VLBI in Europe, PO Box 2, NL-7990 AA, Dwingeloo, The Netherlands*
[3]*Jet Propulsion Laboratory, California Institute of Technology, 4800 Oak Grove Drive, Pasadena, CA 91109, USA*
[4]*Max-Planck-Institut für Radioastronomie, Auf dem Hügel 69, D-53121 Bonn, Germany*

Accepted 2002 February 13. Received 2002 January 3; in original form 2001 July 13

ABSTRACT

A single-screen model of the gravitational lens system 2016+112 is proposed, that explains recent *Hubble Space Telescope* (*HST*) infrared (NICMOS–F160W) observations and new high-resolution European VLBI Network (EVN) 5-GHz radio observations, presented in this paper. In particular, we find that a massive 'dark' structure at the lens position, previously suggested by X-ray, optical and spectroscopic observations of the field around 2016+112, is not necessarily required to accommodate the strong-lensing constraints. A massive structure to the north-west of the lens system, suggested from a weak-lensing analysis of the field, is included in the model. The lensed source is an X-ray bright active galaxy at $z = 3.273$ with a central bright optical continuum core and strong narrow emission lines, suggestive of a type II quasar. The EVN 5-GHz radio maps show a radio jet structure with at least two compact subcomponents. We propose that the diamond caustic crosses the counter-jet of the radio source, so that part of the counter-jet, host galaxy and narrow-line emission regions are quadruply imaged. The remainder of the radio source, including the core, is doubly imaged. Our lens model predicts a very high magnification ($\mu \sim 300$) at the brightness peaks of the inner two radio components of complex C. If the jet exhibits relativistic velocities on microarsecond scales, it might result in apparent *hyperluminal* motion. However, the lack of strong radio variability and the peaked radio spectrum imply that these motions need not be present in the source. Our model furthermore implies that the optical spectrum of C′ can only show features of the active galactic nuclei and its host galaxy.

Key words: gravitational lensing – quasars: general – radio continuum: general.

1 INTRODUCTION

The gravitational lens system 2016+112, discovered by Lawrence et al. (1984), has defied any simple explanation. The system consists of two active galactic nuclei (AGN) images (A and B) at a redshift of $z = 3.273$ (Lawrence et al. 1984; Schneider et al. 1985, 1986), separated by 3.4 arcsec. Early optical and near-infrared (near-IR) observations (e.g. Schneider et al. 1985; Langston, Fischer & Aspin 1991; Lawrence, Neugebauer & Matthews 1993) showed the presence of two extended objects (designated C′[1] and D). C′ lies some 2-arcsec south-east of image B, such that ABC′ nearly form a right-angled triangle. Object D, the primary lens galaxy, has a redshift of 1.01 (Schneider et al. 1985) and is close to the centroid of A, B and C′. The redshift of C′ has resisted measurement. Narrow Lyα emission near A, B and C′ has been detected at a redshift of $z = 3.273$ with linewidths $\lesssim$1000 km s^{-1} (Schneider et al. 1986, 1987; Lawrence 1996; Yamada et al. 2001; Lawrence et al., in preparation). Similarly, two fuzzy patches of Lyα emission were detected about 3 arcsec north-west and west of images A and B, respectively (Schneider et al. 1986, 1987). Recently, high-resolution *F814W*-band (Lawrence et al. in preparation) and F160W-band observations were obtained with the *HST* (see the CASTLES webpage http://cfa-www.harvard.edu/glensdata/MG2016.html; e.g. Muñoz et al. 1998), showing that images A and B are unresolved and compact, whereas C′ is arc-like and does not show obvious compact structure.

At radio wavelengths, 2016+112 has been observed with the Very Large Array (VLA) (e.g. Lawrence et al. 1984; Schneider et al. 1985) and displays three components, A, B and C. All components contain compact substructure in higher-resolution MERLIN (Garrett et al. 1994), very long baseline interferometry (VLBI) (Heflin et al. 1991) and European VLBI Network (EVN) (Garrett et al. 1996) images.

⋆E-mail: leon@tapir.caltech.edu

[1]The prime distinguishes it from the radio structure (designated C), which early on was not known or thought to be associated with the optical emission.

Whereas components A and B consist of at least two subcomponents (oriented approximately north-west), radio component C splits into four dominant subcomponents aligned east–west (e.g. Garrett et al. 1996). Components A and B have steep integrated radio spectra between 18 and 6 cm (Garrett et al. 1994), whereas component C has a somewhat flatter integrated radio spectrum. All component spectra steepen between 6 and 2 cm (Langston et al. 1991). The overall integrated spectrum of the lens system is that of a Gigahertz Peaked Source (GPS) source and peaks somewhere in the range 1–5 GHz. With the VLA in A-array, the source is barely detectable at 22 GHz (Patnaik, private communication). Observations with EVN at 18 cm and MERLIN at 6 cm (Garrett et al. 1996) show that the outermost images (C_{11} and C_2) have significantly steeper spectra than the two innermost components (C_{12} and C_{13}). These observations suggest that the structures $C_{11}+C_{12}$ and $C_{13}+C_2$ have opposite parities and are probably images of the same structure in the source.

Observations of the field around 2016+112 with the *ASCA* satellite X-ray Observatory suggested the presence of diffuse X-ray emission centred on the lens system and to the north-west (Hattori et al. 1997; Benitez et al. 1999). Recent observations with the *Chandra* X-ray Observatory, however, show unambiguously that this emission is mostly a result of discrete sources and not diffuse cluster emission (Chartas et al. 2001). In addition, the lensed images A and B, and complex C′, are detected. The presence of X-ray and narrow emission lines suggests that the source could, in fact, be a type II quasar (e.g. Chartas et al. 2001; Yamada et al. 2001). None of the other X-ray sources in the field are associated with galaxies detected by Soucail et al. (2001, see below). The comparatively large number of X-ray sources in the field of 2016+112 might be the result of a magnification bias, which enhances the number count of sources around the lensing mass distribution if the number density of X-ray source increases steeply at redshifts larger than that of the lens galaxy.

Spectroscopic observations by Soucail et al. (2001) show the presence of an overdensity of galaxies at the same redshift as lens galaxy D. Similarly, Clowe, Trentham & Tonry (2001) detect a 3σ weak-lensing signal to the north-west of the lens system, roughly coincident with the region of excess X-ray emission (e.g. Benitez et al. 1999). The latter could again be caused by a magnification bias. Only a marginal weak-lensing signal at the position of the lens system was found, consistent with the absence of a very massive dark X-ray cluster. If the dispersion in the velocities of the field galaxies, found by Soucail et al. (2001) were representative of a virialized system, one would have expected to see diffuse X-ray emission (Chartas et al. 2001). The absence of the latter therefore also supports the idea that these galaxies have not yet virialized and formed a massive centrally concentrated cluster.

Several models have been proposed to explain these observations. Some employ a single deflector and a single screen (Langston et al. 1991; Benitez et al. 1999), whereas others used more complex models with C′ and D being different galaxies (Narasimha, Subramanian & Chitre 1987). In the proposed two-screen models it is assumed that object C′ is a galaxy at a redshift different from galaxy D, and responsible for lensing radio complex C into additional 'subimages' (Nair 1993; Nair & Garrett 1997). The mirror-symmetry and opposite parities for the structures $C_{11}+C_{12}$ and $C_{13}+C_2$ suggest that the source structure corresponding to complex C is quadruply imaged and that there is no need to invoke a second lens screen, that is not weakly perturbative, but changes the nesting of the caustic curves in the sources plane. However, a two-screen model or a model that has two-lens galaxies in the same lens plane, predicting the same parities as a single-screen single-lens model (Nair & Garrett 1997) can of course not be excluded based on this argument alone.

In this paper we propose an alternative model that can explain these observations quantitatively with a single screen. Instead of explaining the lens system with a complex deflector model, we find it can also be explained by a realistic, although more complex source model. In Section 2, we present EVN 5-GHz radio observations of 2016+112, which suggest that complex C consists of two images with opposite parities. In Section 3, a detailed structure of the source is proposed that can explain qualitatively most of the observed features of the 2016+112 lens system. In Section 4, we present a model of the lens potential that incorporates mass structures from the field around the lens system. In Section 5, we compare the model with the observational constraints to find that it can also explain quantitatively the available observational constraints of the lens system and the field. In Section 6, our results are summarized and discussed. Throughout this paper we assume a flat smooth Friedman–Robertson–Walker (FRW) universe with $\Omega_{\rm m}=0.3$ and $H_0=65$ km s^{-1} Mpc^{-1}.

2 EVN 5-GHZ OBSERVATIONS AND DATA ANALYSIS

The 5-GHz EVN observations were made on 1995 May 17–18 from UT 22:30 to 10:30, using seven antennas of the EVN: the 100-m Effelsberg (DE), 26-m Jodrell Mk2 (UK), 25-m Onsala (SE), 32-m Medicina (IT), 32-m Noto (IT), 32-m Cambridge (UK) and Westerbork array (NL). Technical problems resulted in no data from the latter two antennas. The recording mode was MkIIIa Mode A (56-MHz bandwidth, left-hand circular polarization). A phase-reference observing scheme was used, switching between the target, 2016+112, and a compact calibrator, J2029+121, located 1° away. The tape ran continuously through each 13 min pass, and the source-switching cycle consisted of alternating between 90 s on the calibrator and 140 s on the target. Correlation of the data was conducted at the MPIfR MkIIIa correlator in Bonn. To prevent loss of data during correlator synchronization of the very short scans, each baseline was correlated twice as a continuous tape pass, once at each of the two source positions. (Spurious correlations on the 'wrong' source were edited out in the later data analysis.)

Subsequent data processing and analysis was performed with the NRAO AIPS package. Long fringe-fitting solutions were made that included several switching phases of the calibrator; the resulting phase, delay and rate solutions were then applied to 2016+112. Although the interferometer model used in the MPIfR correlator was not sufficiently accurate to permit direct phase-referencing, this process did remove short-term phase fluctuations, and allowed longer solution intervals to be used for self-calibration of the phases of the 2016+112 visibilities. Amplitude calibration was made by initially assuming that J2029+121 is a 0.91-Jy point source on all baselines, and then determining self-calibration corrections after mapping the source. These amplitude and phase corrections were also applied to 2016+112. In order to prevent fringe-rate and delay smearing over the 4-arcsec field of view, the data associated with 2016+112 were maintained as 28 contiguous 2-MHz channels with a visibility averaging time of 2.5 s. The calibrated 2016+112 data were Fourier transformed and a naturally weighted, tapered image of the full field was produced. All three main regions of emission A, B and C were clearly detected and the image was used as an input model for subsequent (phase-only) self-calibration. Since 2016+112 is a rather faint, resolved radio source, improvements to the original phase solutions were only obtained by employing a relatively long solution

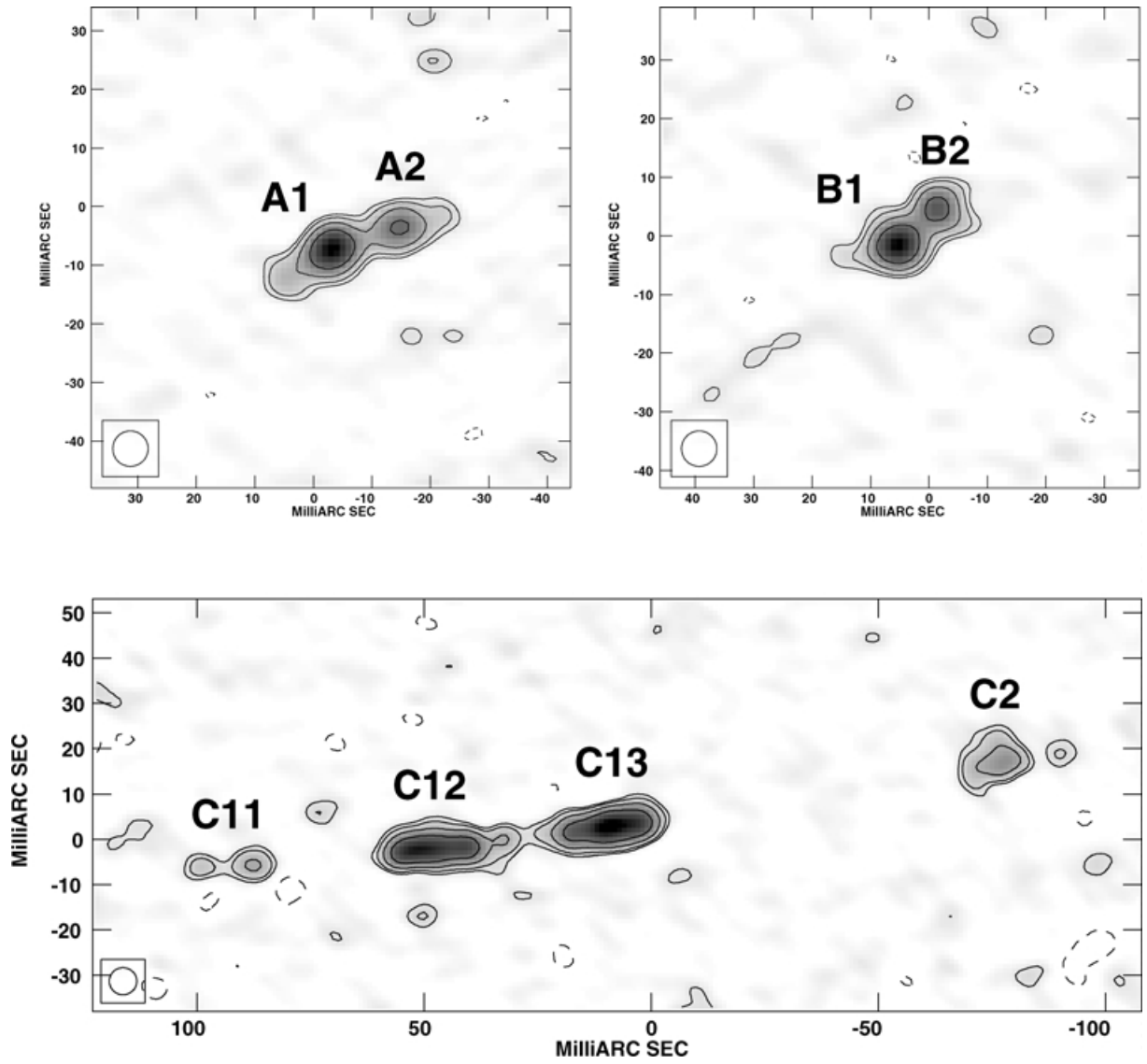

Figure 1. European VLBI Network 5-GHz radio images of regions A, B and C of 2016+112. Contour levels indicate (−3, 3, 5, 10, 20) times the rms noise level of 0.14 mJy beam^{-1}. Note the jet-like substructure in images A and B, and the apparent 'mirror-symmetry' of components C_{12} and C_{13}, suggesting opposite parties due to lensing. The model proposed in this paper assumes that both components are images of a quadruply lensed part of the source, which is associated with the counter-jet in components A_2 and B_2, the core of the source. Components C_{11} and C_2 are presumably steep-spectrum images of intrinsically faint (but highly magnified) substructure further along the counter-jet (i.e. west of A_2 and B_2). The restoring beam has a FWHM of 6 milli-arcsec.

interval (13 min) over the entire frequency band (56 MHz). CLEANed maps of the three main regions of emission are presented in Fig. 1. All the maps are naturally weighted (the rms noise level is ∼140 μJy beam^{-1}) and the FWHM of the circular restoring beam is 6 mas.

To obtain the positions and flux densities of the radio components in regions A, B and C, elliptical Gaussians were fitted to the images. Images A and B were fitted by two Gaussians. Images C_{12} and C_{13} could not be fitted by single elliptical Gaussians and were therefore each fitted by two Gaussians (*a* and *b*, respectively). The results of these fits are listed in Table 1.

3 THE SOURCE

Based on the optical/infrared (IR) and radio observations of 2016+112 (see Sections 1 and 2), we postulate the following simple picture for the lensed source (see also Langston et al. 1991; Benitez et al. 1999, for analogous models). First, we assume that optical continuum emission of images A and B is from an AGN (possibly a type II quasar) near the core of some faint underlying host galaxy, which is not detected at A and B owing to its very low surface brightness compared with the AGN. Secondly, the NW elongation of the EVN 1.7-GHz radio images of A and B (Garrett et al. 1996), is now confirmed by the high-resolution EVN observations at 5 GHz presented in Section 2, showing that both components consist of at least two subcomponents. We assume that the flatter-spectrum subcomponents seen at 5 GHz (A_2 and B_2) are associated with the optical continuum core and the other two (A_1 and B_1) are jet-features. Because the constraints from the optical emission are not used at this level of positional accuracy (few mas), this particular choice is of little relevance for the lens modelling.

Additionally, strong spectral lines (e.g. Lyα, C IV, N V, Si IV) are seen near images A, B and C′ (e.g. Schneider et al. 1986, 1987;

Table 1. Properties of the image components determined from the 5-GHz EVN data (Section 2). Column 1: the mane of the component as in Garrett et al. (1996). Columns 2–3: the positions determined from Gaussian fits to the 5-GHz EVN images. The positional error is 1 mas with respect to A_1. Column 4: the total flux density and error on the last significant digit (within parentheses) of each of the components. Column 5: the position angles (PA) of the presumed jet direction, measured in the direction $A_1 \rightarrow A_2, B_1 \rightarrow B_2$, $C_{12b} \rightarrow C_{12a} \rightarrow C_{11}$ and $C_{13b} \rightarrow C_{13a} \rightarrow C_2$ from north to east. Column 6: the parities $p_{\pm}$, based on general assumption of the source structure and geometry of the time-delay surface (e.g. Blandford & Narayan 1986).

Comp.	RA (arcsec)	Dec (arcsec)	$S_{5\,\mathrm{GHz}}$ (mJy)	PA (deg)	$p_{\pm}$
A_1	+0.0000	+0.0000	8.0(0.3)	−71.7	+
A_2	−0.0121	+0.0040	4.5(0.3)	–	+
B_1	−3.0057	−1.5040	7.3(0.3)	−48.5	−
B_2	−3.0126	−1.4979	4.2(0.3)	–	−
C_{11}	−2.0111	−3.2331	1.9(0.3)	–	−
C_{12a}	−2.0455	−3.2300	3.8(0.3)	+95.1	−
C_{12b}	−2.0542	−3.2294	13.9(0.5)	+93.9	−
C_{13a}	−2.0937	−3.2241	8.7(0.4)	−80.2	+
C_{13b}	−2.0855	−3.2254	9.8(0.4)	−81.0	+
C_2	−2.1749	−3.2101	5.6(0.5)	–	+

Lawrence 1996; Yamada et al. 2001). However, the linewidths are very narrow compared with a typical quasar spectrum drawn from the same redshift range (see Steidel, Pettini & Adelberger 2001). This is a puzzle, although it could be that line emission from the BLR is obscured, as suggested by Yamada et al. (2001), and that only the NLR further from the core is seen. This would also explain why the Lyα emission is not exactly coincident with A, B and C′, but offset from C′ by 1 WFPC2 pixel (0.0455 arcsec) when aligned with A and B. These narrow-line spectra are indicative of a type II quasar (Yamada et al. 2001), which is supported by the X-ray brightness of the source (Chartas et al. 2001). A schematic picture of the source is shown in Fig. 2.

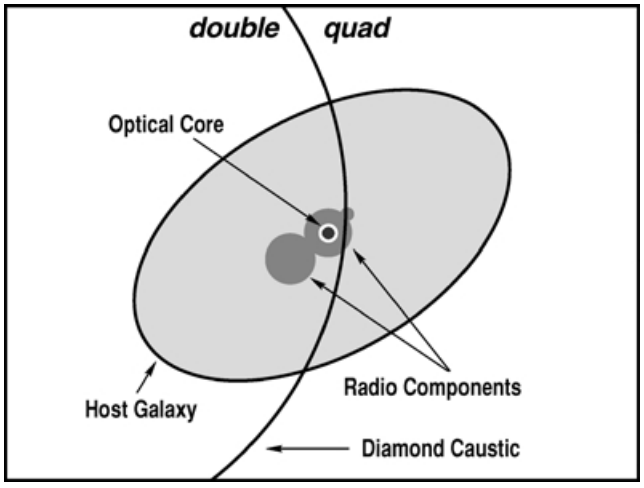

Figure 2. A schematic view of the proposed source structure for 2016+112. The AGN, associated radio core, part of host galaxy and the second radio component are doubly imaged. The western-most part of the radio core and part of the host galaxy are quadruply imaged. The components are not drawn to scale, nor do the ellipticity and position angles of host galaxy and other structures necessarily represent those of the true underlying source.

Qualitatively, this source structure can explain both the optical and radio data of 2016+112 available to date, if the diamond caustic (fold) crosses the source as indicated in Fig. 2: (i) the optical core is doubly imaged at A and B, because it falls outside the diamond caustic; (ii) most of the associated radio structure is also doubly imaged near A and B; (iii) only part of the radio structure, associated with the counter-jet near radio subcomponents A_2 and B_2, is quadruply imaged, such that C_{12} and C_{13} are fainter than what one might expect based on their proximity to the critical curve (i.e. the high magnification) and the flux density of A_2 and B_2; (iv) components C_{11} and C_2 are steep-spectrum emission further along the counter-jet, which are quadruply imaged but only detected near C because of the very high magnification near the critical curve; (v) part of the underlying host galaxy is doubly imaged, but is too faint to be seen at images A and B as a result of the bright AGN emission (and its associated point spread function); (vi) the other part of the host galaxy is quadruply imaged, resulting in the highly magnified arc (i.e. complex C′); (vii) similarly the extended Lyα emission (Lawrence et al., in preparation), as well as the narrow-line emission in general (e.g. Yamada et al. 2001), is expected to surround the optical core and is part doubly and part quadruply imaged (i.e. that part inside the diamond caustic) and therefore seen near A, B and C′. This is supported by the idea that the emission-line ratios near C′ are more consistent with it originating further from the core (Yamada et al. 2001). Although the proposed model might appear very complicated, it is precisely the complex lensed structure one expects from AGNs – which have abundant wavelength-dependent structure on subarcsec scales – if they happen to cross a caustic.

Support for the suggestion that part of the radio source crosses the caustic is given by the actual 'merger' of radio components C_{12} and C_{13} at the few-σ level of the surface brightness contours in Fig. 1. This *only* occurs if part of the source at that surface brightness level actually crosses the caustic in the source plane. The critical curve crosses precisely that point in the image plane where the two images merge [i.e. the 'saddle point' in the surface brightness distribution between C_{12} and C_{13}; see, e.g., Kochanek, Keeton & McLeod (2001)]. Owing to the conservation of surface brightness in gravitational lensing, we expect the point where images C_{12} and C_{13} merge to be associated with extended structure north-west of A_2 and B_2 at the few-σ contour level as well (see Fig. 1). Images C_{12} and C_{13} are associated with very compact (i.e. a few μ as) substructure in the counter-jet, which unfortunately is barely observable near images A and B, owing to their relatively low magnifications (see Section 5 below) and of course the finite resolution of the observations. This is even more strongly the case for the faint and steep-spectrum emission from C_{11} and C_2.

In the model by Langston et al. (1991) the second flat-spectrum source component (i.e. the component associated with A_2 and B_2) lies almost fully *inside* the diamond caustic, whereas the steeper spectrum component straddles the caustic. Nair & Garrett (1997) showed, however, that this particular model predicts the inner two images of complex C to be a steep spectrum and the outer two flat spectrum, in contrast to observations. On this basis, the model from Langston et al. (1991) was rejected. In the model proposed here, however, the steeper spectrum component lies fully *outside* the diamond caustic, whereas only a small part of the flat-spectrum component straddles the caustic from the outside. This small part (i.e. the counter-jet) inside the caustic is quadruply imaged and highly magnified, creating images C_{12} and C_{13}. Note that the direction of merging images C_{12} and C_{13} is perpendicular to the caustic near the source position (Fig. 3 below), as must generally be true for a single-screen model (Blandford & Narayan 1986). Further inside

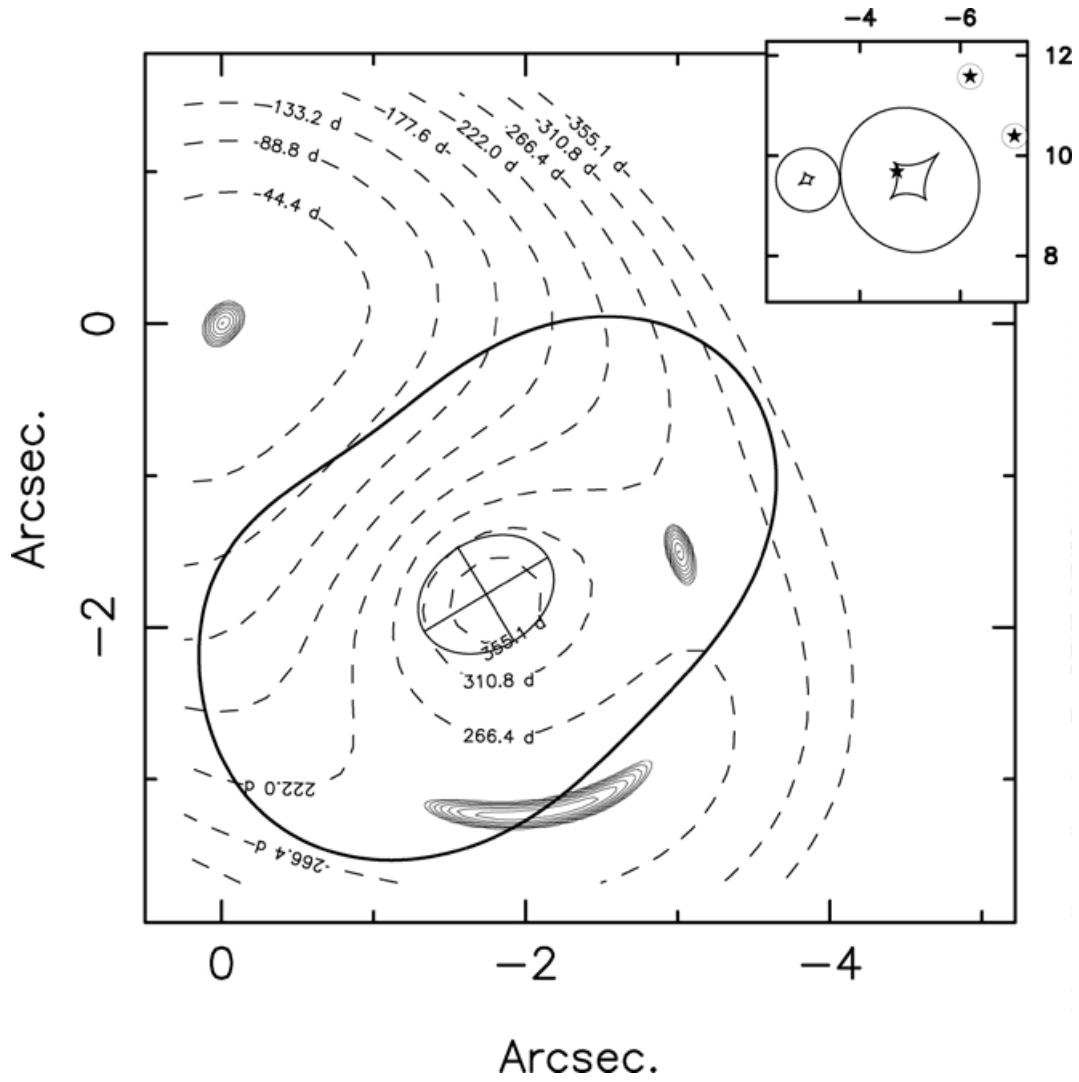

Figure 3. The model of 2016+112 as indicated in Table 3, assuming M_2 is an L_* galaxy with $\sigma_{||} = 225$ km s^{-1} at $(-3.2, -0.4)$ arcsec from image A. The thick line indicates the critical curve. The ellipse indicates the position, flattening and position angle of the primary lens galaxy (i.e. D), whereas the dashed lines indicate constant time-delay contours. The subpanel (units in arcsec) shows the caustics of galaxies D and M_2, the source (indicated by the star inside the caustics) and the two Lyα patches (stars with circles; see Section 6). The caustics are displaced to the north from the primary lens galaxy by $\sim$10 arcsec owing to a massive structure M_1, inferred from weak lensing (see text).

the caustic, we postulate that the spectrum of the counter-jet steepens and that a small subcomponent is lensed into images C_{11} and C_2. Both of these are only seen near C, because of their exceedingly high magnifications (Section 5).

This type of lens-source configuration is not uncommon. Several radio gravitational lens systems have been observed with part of the source inside and part of the source outside the diamond caustic (e.g. Einstein rings). In particular, the JVAS/CLASS lens B1938+666 has a radio jet structure crossing the diamond caustic near the cusp, although in this case most of the source lies inside the caustic (King et al. 1997), whereas in 2016+112 only the counter-jet is quadruply imaged.

The question is now whether we can also *quantitatively* explain the *primary constraints* [e.g. radio and optical image positions, the jet position angles (PA) and the flux-density ratios], and whether the resulting model is in agreement with *secondary constraints*, such as the properties of the host galaxy (D) and the detection of one or more nearby mass concentrations in weak-lensing (Clowe et al. 2001) and spectroscopic studies (Soucail et al. 2001).

4 THE LENS AND FIELD

First, we associate a singular isothermal elliptical (SIE) mass distribution (e.g. Kassiola & Kovner 1993; Kormann, Schneider & Bartelmann 1994; Keeton, Kochanek & Seljak 1997) with the primary lens galaxy D, although a mass model with a steeper or more shallow mass profile is not a priori excluded (e.g. Benitez et al. 1999). In light of the present uncertainties, especially concerning external perturbers, we feel it is not yet warranted to explore more detailed lens mass models. We associate the centre of the mass distribution (MD) with the centroid of the surface brightness distribution (SBD) of galaxy D, measured from the *HST* NICMOS F160W-band image (CASTLES; e.g. Muñoz et al. 1998), i.e. $(-1.740 \pm 0.003, -1.782 \pm 0.003)$ arcsec with

respect to image A. In general, good agreement is found between position angles of the SBD and MD of lens galaxies (Keeton et al. 1997). To avoid underconstraining the mass model, we have chosen to fix the position angle of the MD at the observed SB value of $-59^\circ \pm 2^\circ$ (see the CASTLES web page). The only free parameters of the MD of lens galaxy D are therefore the axial ratio (f) and the central velocity dispersion ($\sigma_{||}$; as defined in Kormann et al. 1994).

To model the surrounding field, we place a singular isothermal sphere (SIS) mass distribution (designated M_1) at the position (−24.0, +60.0) arcsec NW of image A, where Clowe et al. (2001, see Section 1) find a significant weak-lensing signal. A SIS fit to the weak-lensing shear field suggests a velocity dispersion of 970^{+150}_{-180} km s^{-1} (1σ errors; assuming a redshift of unity). We constrain the velocity dispersion of M_1 to this value. In addition, Soucail et al. (2001) have spectroscopically confirmed the presence of an overdensity of at least six in red galaxies at the redshift of lens galaxy D. They estimate a velocity dispersion of 771^{+430}_{-160} km s^{-1}. Clowe et al. (2001) do not to find a strong shear signal at this position ($\sigma = 560^{+220}_{-480}$ km s^{-1}; 1σ errors). The low signal-to-noise ratio of the observations, however, does not allow one to exclude it. We include this mass distribution to first order by modelling it as an SIS (M_2). This is done in order to test whether an additional mass distribution is indeed required by the strong-lensing constraints, as suggested by these previous authors. We allow the velocity dispersion of M_2 to vary between 560 and 175 km s^{-1} and let its position be free. The upper limit is roughly defined, such that M_2 does not result in additional observable images of the background source, although this constraint could be lifted if this mass distribution has a large finite core and is not capable of multiple imaging. Similarly, the lower limit avoids additional subimages of A, when M_2 nearly coincides with its position (see Section 5). In the latter case, the velocity dispersion of M_2 is of galactic scale (a few hundred km s^{-1}), in which case the core radius is typically small. We include an external shear with both its strength and positional angle as free parameters.

4.1 Constraints

As primary constraints on this starting model, we use the observed properties of images A, B, C_{12} and C_{13}, as found from the *HST* NICMOS F160W-band (e.g. CASTLES) and EVN 5-GHz images (Section 2; Table 1). The relative positions of A and B in the optical and radio bands agree to within the measurement errors. There appears to be a slight offset in declination between the F160W-band emission of complex C′ in the *HST* image and the positions of the EVN radio components. It amounts, however, to only 1 pixel (0.1 arcsec) and in light of the uncertain structure of the host galaxy, we consider this difference unimportant at present. The optical brightness ratio between images A and B, found from the *HST* NICMOS F160W-band image is $r_n = 0.97 \pm 0.02$ (i.e. S_B/S_A). Garrett et al. (1996), however, find $r_n = 0.84 \pm 0.01$ at 1.7 GHz. We therefore adopt an 'average' value $r_n = 0.90 \pm 0.10$ for the flux ratio between images A and B, in our lens modelling, where the uncertainty accounts for possible variability, even though the source does not appear to vary strongly (Haarsma et al. 2001). The adopted value is also consistent with $r_n = 0.92 \pm 0.05$ found from the EVN 6-cm observations, presented in this paper (Table 1).

We do not use the positions of images C_{11} and C_2 as constraints. According to the source model (Section 3; Fig. 2), they are part of the source structure associated with lensed images A_2 and B_2. They appear somewhat more resolved in the EVN 5-GHz observations (Section 2), although the signal-to-noise ratio is low, and have steeper spectra compared with the other images between the EVN at 1.7 and 5 GHz. Hence, they are probably not part of the same region of the source that is responsible for images A_2, B_2, $C_{12a/b}$ and $C_{13a/b}$ seen in Fig. 1. The emission from C_{11} and C_2 most probably originates further along the counter-jet, which presumably has a steeper spectrum (Section 3). We assume that the emission from C_{12a} and C_{13a} is associated with structure of the unresolved images A_2 and B_2, within a 1-mas radius from their respective centroids. Although this particular choice might seem arbitrary, it is probably conservative based on the notion that from an inverse Compton limit on the brightness temperature of these radio sources, between 10^{11} and 10^{12} K, a component size for A_2 and B_2 as small as 0.1–0.3 mas can be expected, given their observed flux densities. If the axial ratios of the components are large (i.e. jet-like), the emission region could easily 'stretch' to 1 mas or larger in one direction. We do *not* use the flux-density ratios between images A_2, B_2 and complex C, because the source structure lies on a caustic and consequently has a strong magnification gradient over its extent. The source can therefore not be treated as a point source, rendering the use of a flux-density ratio very difficult. All constraints are listed in Table 1.

5 RESULTS

Using the mass model and the constraints discussed above, we vary the nine free parameters using the simulated annealing downhill simplex method described in Press et al. (1992), until the differences between the observed and recovered image properties are minimized in terms of the χ^2-value (goodness of fit). Using different starting values of the parameters, we ensure that the final solution is close to the absolute minimum in χ^2-space.

We vary the velocity dispersion of M_2 between 560 and 175 km s^{-1} (see above) and minimize χ^2 for the other free parameters. The goodness-of-fit χ^2 (for two degrees of freedom) of the best models increases only marginally between these upper and lower limits on the velocity dispersion of M_2, i.e. from 1.1 to 1.5, respectively. This indicates a strong degeneracy in the lens model, between the velocity dispersion and position of M_2 and the external shear. The velocity dispersion and axial ratio of G1 are only marginally affected. We note that the χ^2-values cannot be used to calculate a likelihood for the model, because we did not strictly use measurement errors for all constraints. The image positions, flux ratio, PAs and parities are recovered in good agreement with the constraints (Table 1), given the uncertainties in the structure of the lensed images. The recovered image properties, inferred magnifications and time delays are listed in Table 2. In Fig. 3, we show the image configuration, critical curve, caustics and time-delay surface of this model.

In Table 3, we have listed the recovered parameters of the lens galaxy D and two additional mass structures M_1 and M_2. We find that the SD axial ratio $f = 0.75$–0.76 of galaxy D is somewhat larger than that determined from its SB distribution, i.e. 0.57 ± 0.01, as seen in the *HST* NICMOS–F160W observations (e.g. see the CASTLES web page; see also Benitez et al. 1999). The velocity dispersion of 320–340 km s^{-1} of galaxy D implies a rest-frame mass-to-light ratio of $(M/L)_H \approx 1.7 h_{65}\, M_\odot/L_{H,\odot}$ (no evolutionary correction), assuming a singular isothermal sphere to calculate the mass inside the Einstein radius, an F160W-band magnitude for lens galaxy D of 18.12 ± 0.04 (see the CASTLES web-page) and the galaxy models from Poggianti (1997). This mass-to-light ratio compares well with those found for other lens galaxies (e.g. Jackson et al. 1998), which indicates that the image separation should not be significantly affected by a mass contribution with a different mass-to-light ratio

Table 2. Recovered image parameters (see Table 1). The flux ratios and magnifications (assuming point-source structures) are given by $r_{\{B,C\}/A}$ and μ, respectively, and the time-delays are given by Δt with respect to the leading image A_1 (assuming the cosmological model mentioned in Section 1). The first and second values indicate those for $\sigma_{M1} = 560$ and 175 km s^{-1}, respectively. The recovered source positions for $\{A_1, B_1\}$ and $\{A_2, B_2, C_{12b}, C_{13b}\}$ are (1.214/5.010, 10.143/9.670) arcsec and (1.220/5.003, 10.144/9.669) arcsec, respectively. Even though, the change in source position is large, when changing σ_{M1}, this is of no relevance because it not an observable.

Comp.	RA (arcsec)	Dec (arcsec)	$r_{\{B,C\}/A}$	μ	$\Delta t/h_{65}$ (d)
A_1	+0.0008/0.0008	−0.0002/0.0000	[1.0]	+4.0/3.3	≡0.0
A_2	−0.0121/0.0121	+0.0040/0.0040	[1.0]	+4.0/3.3	3.3/9.1
B_1	−3.0060/3.0060	−1.5036/1.5033	0.91/0.85	−3.6/2.8	255.3/291.6
B_2	−3.0126/3.0127	−1.4979/1.4981	0.90/0.84	−3.6/2.8	254.9/286.4
C_{12b}	−2.0542/2.0542	−3.2294/3.2292	91.8/77.4	−367/252	224.1/254.6
C_{13b}	−2.0855/2.0855	−3.2254/3.2257	92.5/78.2	+369/255	224.1/254.6

Table 3. The fixed (between brackets) and reconstructed mass-model parameters for the primary lens galaxy D and the two SIS mass distributions M_1 and M_2. The arrows indicate how the values change as the velocity dispersion of M_2 is lowered from 560 to 175 km s^{-1}. In addition to the mass distributions, an external shear (γ_{ext}) is found with strength 0.12 → 0.07 and position angle −24° → −51°.

Defl.	RA (arcsec)	Dec (arcsec)	f	PA (deg)	$\sigma_{\|\|}$ (km s^{-1})
D	[−1.740]	[−1.782]	0.75–0.77	[−59]	320 → 342
M_1	[−24.0]	[+60.0]	[1.0]	[0.0]	[970]
M_2	11.6 → 2.0	0.8 → −0.4	[1.0]	[0.0]	[560] → [175]

(e.g. a dark cluster). In that case, the lens galaxy would most probably not have been on the fundamental plane of early-type galaxies either (Kochanek et al. 2000).

The model also indicates the presence of an external shear with a strength γ between 0.07 and 0.12 and a position angle between −24° and −51° depending on the velocity dispersion of M_2. If we investigate the *I*-band image (fig. 2 in Soucail et al. 2001) in more detail, there appears to be a 'filamentary structure' of high-redshift galaxies running across the lens system. This 'filament' is *not* dynamically related, because it contains galaxies over a very different range of redshifts ($z \approx 0.6$–1.1), but it might be responsible for the shear at the position of 2016+112. On the other hand, the closeness of the position angle of the external shear and that of the SB of galaxy D, for low-velocity dispersions of M_2, might also indicate that either the mass distribution of galaxy D has a different radial mass profile or that its flattening is a function of radius.

Finally, we note the remarkably high magnification ($\mu \sim 300$) at the brightness peaks (i.e. not integrated over the image) of images C_{12} and C_{13}, although the precise value is sensitive to the details of the model input (see also below). For example, the magnification changes by about ∼10 per cent when changing the slope of the radial mass profile by ∼5 per cent. Even so, this is the highest (inferred) magnification for any known lens system. Because it is primarily directed tangentially and the jet direction is nearly perpendicular to the fold caustic, according to the model, any relativistic motion in the radio jet structure will be enhanced by a factor of $\sim\mu$. Superluminal velocities of say $\sim 3h^{-1}c$ (e.g. Vermeulen & Cohen 1994) could therefore lead to *hyperluminal* velocities of $\sim 10^3\, h^{-1}c$. Similarly, one can probe structure on intrinsic scales of a few microarcsec when observed with VLBI. On the other hand, if the lensed structure is part of the counter-jet (see Section 3), such high velocities are no longer expected (even though velocities of $\sim 0.5h^{-1}c$ for the counter-jet are still likely and could lead to *hyperluminal* velocities of $\sim 10^2\, h^{-1}c$). The absence of strong variability in the source (Haarsma et al. 2001) and its GPS-type radio spectrum might, however, be indicative of the absence of strongly relativistic motion.

One problem that we have not yet addressed is the considerable difference in angular distance between the pair components C_{11}–C_{12} and C_{13}–C_2, which we did not include in the lens model. Given the high magnification and symmetry around the critical curve, one would expect these distances to be similar. The fact that they are not similar seems to argue against our model and in favour of a two-lens model (Nair & Garrett 1997). However, magnifications and the magnification matrix are a function of differences in higher-order derivatives of the local lens potential (see Schneider, Ehlers & Falco 1992). Especially in regions of very high magnification, many of these derivatives are very close to zero, because in those cases the lensed images form at very shallow extrema of the time-delay surface (e.g. Blandford & Hogg 1996). It is therefore not inconceivable that even a miniscule perturbation of the local lens potential (e.g. by a globular cluster, halo substructure, etc.) will have an enormous effect on the local magnification matrix, i.e. on the image magnifications and the image positions. These discrepancies near critical curves have been seen in other lens systems with very high image magnifications (Mao & Schneider 1998) and might not be uncommon in general. As an example, if we include a typical globular cluster with a velocity dispersion $\sigma = 7$ km s^{-1} (Einstein radius of $\lesssim$1 mas) about 5 mas away from image C_2, it changes the magnifications of C_2 and C_{11} considerably, but also projects them on the same position in the source plane. The magnification ratio between C_{12} and C_{13} remains equal to unity within a few per cent. The probability of such minor perturbations is considerable, especially because one expects hundreds if not thousands of globular clusters, dwarf satellites, etc. around these massive elliptical galaxies. At higher redshift, according to cosmological cold dark matter models, the amount of halo substructure could be even more prevalent. We are therefore not too worried about this apparent discrepancy, but are warned that even though the magnifications in complex C are very high, their precise values are quite uncertain and should only be taken as indicative.

6 DISCUSSION AND CONCLUSION

We have shown that 2016+112 can be explained by a *single-screen* mass model. The observational constraints are reasonably well reproduced by the proposed model. The axial ratio of the surface

MD of the lens galaxy D is somewhat larger than the axial ratio of its SB distribution, as determined from *HST* NICMOS F160W-band observations. Also its mass-to-light ratio is in good agreement with that of other lens galaxies. Surprisingly, our model is consistent with the presence of a massive component about 1-arcsec north–west of the lens galaxy, suggested from a weak-lensing analysis of the field (Clowe et al. 2001). We find evidence for an external shear that might result from a 'filamentary structure' of high-redshift galaxies running across the lens system roughly from east to west (see Soucail et al. 2001). This filament is not a dynamically related structure, because it contains galaxies over a wide range of redshifts. The massive dark cluster previously suggested cannot be confirmed or excluded, based on the strong-lensing constraints. In particular, a single $\sim L_*$ galaxy several arcsec east of galaxy D (see Fig. 3) could also be consistent with the strong-lensing constraints. A faint object at that approximate position does appear on a deep *R*-band image, i.e. fig. 4 in Clowe et al. (2001), although we do not know whether that object is indeed a galaxy and what redshift is has (i.e. whether it forms a second lens screen). Given the high redshift of the source, a perturbing galaxy at that position could have a wide range of redshifts (0.5–1.5), not necessarily being that of the primary lens galaxy.

Because we can explain the available data on 2016+112 with a single-screen model, we conclude that a second screen is at most only a perturbation and that the optical/IR object C′ is a highly magnified arc of the AGN host galaxy at $z = 3.273$. Thus, we predict that optical spectroscopy of complex C′ will not yield a redshift in between that of the lens galaxy D and the source as previously suspected, but will instead *only* show features at the source redshift.

Our model predicts a very high magnification ($\mu \sim 300$) at the brightness peaks of images C_{12} and C_{13}. This can be expected based on the proximity of these images (only ∼20 mas; see Fig. 1) to the critical curve passing in between them. Because, the magnification is inversely proportional to the separation between the two images (e.g. Schneider et al. 1992, Chapter 6), the small separation (∼40 mas) between the images results in an order of magnitude higher magnification than normally observed. This is enhanced by the small angle between the line joining the images and the caustic, resulting in an even smaller distance of the images to the caustic (i.e. a higher magnification). A magnification that is one to two orders of magnitude larger than normally seen for two merging images ($\mu \sim 10$), can therefore be expected. This magnification could lead to observable *hyperluminal* motion with velocities of the order of $\sim 10^3 h^{-1} c$ of microarcsec-scale structure in the lensed jet, although the GPS-type radio spectrum and low variability of the source at present do not support the notion of high apparent velocities in the radio jet, especially also because our model suggests that it is the counter-jet that is being magnified.

Our source model appears to be that of a type II quasar (e.g. Yamada et al. 2001; Chartas et al. 2001). At radio wavelengths, only the counter-jet of the source is quadruply imaged, whereas the AGN core and radio jet are doubly imaged. The host galaxy and the extended narrow-line emission around the core is part doubly and part quadruply imaged, which explains its offset from the optical and radio structures and also the difference in line ratios between images A and B, and complex C (Yamada et al. 2001). The absence of BLR emission and the presence of X-ray emission (Chartas et al. 2001) further support the identification of this source as a type II quasar.

Finally, we suggest that the two patches of Lyα emission found by Schneider et al. (1986, 1987) could be cold gas clouds in the intergalactic medium (IGM) – possibly around some nearby galaxies – that are illuminated by the emission cone coming from the AGN along the jet axes. There are indeed several objects at the positions of these patches (Clowe et al. 2001; Soucail et al. 2001), of which the brightest has the same redshift as the source (Soucail et al. 2001). When projecting the two patches on the source plane (Fig. 3), using the mass model presented in this paper, we find that one lies close to the (counter) jet axis in the source plane, i.e. ∼20°, whereas the second patch makes an angle of ∼50°. Their distances to the AGN in the source plane are 1.9 and 1.5 arcsec, respectively. They are therefore not multiply imaged. If the jet is pointed towards (or away from) the observer, the real angles between the patch, AGN and observer could be smaller. The low expected metallicity for such IGM clouds could explain the presence of strong Lyα emission lines and the absence of strong metal lines, such as the C IV lines seen near images A, B and C′ (Schneider et al. 1987; Lawrence 1996). If these patches are indeed illuminated by the AGN, we expect this Lyα emission to be highly polarized. Polarimetry observations on a 10-m class telescope could confirm this.

The ultimate test between the different one- and two-lens models will be the measurement of the redshift of spectral (emission and absorption) lines from complex C′, which can only be $z \approx 3.273$, according to the model proposed in this paper.

ACKNOWLEDGMENTS

The European VLBI Network is a joint facility of European and Chinese radio astronomy institutes funded by their national research councils. LVEK and RDB would like to thank Ian Browne for invaluable help during the initial phases of this research. We thank Ian Browne and Sunita Nair for useful comments on a draft of the paper. LVEK thanks Eric Agol for stimulating discussions and George Chartas for sending a version of their paper on *Chandra* X-ray observations of 2016+112 prior to publication. This research has been supported by NSF AST-9900866 and STScI GO-06543.03-95A.

REFERENCES

Benitez N., Broadhurst T., Rosati P., Courbin F., Squires G., Lidman C., Magain P., 1999, ApJ, 527, 31
Blandford R. D., Hogg D. W., 1996, in Proc. IAU Symp. Vol. 173, Astrophysical Applications of Gravitational Lensing, p. 355
Blandford R., Narayan R., 1986, ApJ, 310, 568
Chartas G., Bautz M., Garmire G., Jones C., Schneider D. P., 2001, ApJ, 550, L163
Clowe D., Trentham N., Tonry J., 2001, A&A, 369, 16
Garrett M. A., Muxlow T. W. B., Patnaik A. R., Walsh D., 1994, MNRAS, 269, 902
Garrett M. A., Porcas R. W., Nair S., Patnaik A. R., 1996, MNRAS, 279, L7
Haarsma D. B., Hoekema K. J., Hewitt J. N., Langston G. I., 2001, American Astronomical Society Meeting, 198, 3703
Hattori M. et al., 1997, Nat, 388, 146
Heflin M. B., Gorenstein M. V., Lawrence C. R., Burke B. F., 1991, ApJ, 378, 519
Jackson N., Helbig P., Browne I., Fassnacht C. D., Koopmans L., Marlow D., Wilkinson P. N., 1998, A&A, 334, L33
Kassiola A., Kovner I., 1993, ApJ, 417, 450
Keeton C. R., Kochanek C. S., Seljak U., 1997, ApJ, 482, 604
King L. J., Browne I. W. A., Muxlow T. W. B., Narasimha D., Patnaik A. R., Porcas R. W., Wilkinson P. N., 1997, MNRAS, 289, 450
Kochanek C. S. et al. 2000, ApJ, 543, 131
Kochanek C. S., Keeton C. R., McLeod B. A., 2001, ApJ, 547, 50
Kormann R., Schneider P., Bartelmann M., 1994, A&A, 284, 285
Langston G., Fischer J., Aspin C., 1991, AJ, 102, 1253

Lawrence C. R., 1996, in Proc. IAU Symp. 173, Astrophysical Applications of Gravitational Lensing. Kluwer, Dordrecht, p. 299
Lawrence C. R., Schneider D. P., Schmidt M., Bennett C. L., Hewitt J. N., Burke B. F., Turner E. L., Gunn J. E., 1984, Science, 223, 46
Lawrence C. R., Neugebauer G., Matthews K., 1993, AJ, 105, 17
Mao S., Schneider P., 1998, MNRAS, 295, 587
Muñoz J. A., Falco E. E., Kochanek C. S., Lehár J., McLeod B. A., Impey C. D., Rix H., Peng C. Y., 1998, Ap&SS, 263, 51
Nair S., 1993, Bull. Astron. Soc. India, 21, 425
Nair S., Garrett M. A., 1997, MNRAS, 284, 58
Narasimha D., Subramanian K., Chitre S. M., 1987, ApJ, 315, 434
Poggianti B. M., 1997, A&ASS, 122, 399
Press W. H., Teukolsky S. A., Vetterling W. T., Flannery B. P., 1992, Numerical Recipes in C. The Art of Scientific Computing. Cambridge Univ. Press, Cambridge
Schneider D. P., Lawrence C. R., Schmidt M., Gunn J. E., Turner E. L., Burke B. F., Dhawan V., 1985, ApJ, 294, 66
Schneider D. P., Gunn J. E., Turner E. L., Lawrence C. R., Hewitt J. N., Schmidt M., Burke B. F., 1986, AJ, 91, 991
Schneider D. P., Gunn J. E., Turner E. L., Lawrence C. R., Schmidt M., Burke B. F., 1987, AJ, 94, 12
Schneider P., Ehlers J., Falco E. E., 1992, Gravitational Lenses, Vol. XIV. Springer-Verlag, Berlin
Soucail G., Kneib J.-P., Jaunsen A. O., Hjorth J., Hattori M., Yamada T., 2001, A&A, 367, 741
Steidel C. C., Pettini M., Adelberger K. L., 2001, ApJ, 546, 665
Vermeulen R. C., Cohen M. H., 1994, ApJ, 430, 467
Yamada T., Yamazaki S., Hattori M., Soucail G., Kneib J.-P., 2001, A&A, 367, 51

This paper has been typeset from a TEX/LATEX file prepared by the author.